Quad-LED and Dual-LED Complex Modulation for Visible Light Communication

T. Lakshmi Narasimhan[†], R. Tejaswi, and A. Chockalingam

† Presently with Department of EECS, Syracuse University, Syracuse, NY 13244, USA

Department of ECE, Indian Institute of Science, Bangalore 560012

Abstract—In this paper, we propose simple and novel complex modulation techniques that exploit the spatial domain to transmit complex-valued modulation symbols in visible light wireless communication. The idea is to use multiple light emitting diodes (LEDs) to convey the real and imaginary parts of a complex modulation symbol and their sign information, or, alternately, to convey the magnitude and phase of a complex symbol. The proposed techniques are termed as *quad-LED complex modulation (QCM)* and *dual-LED complex modulation (DCM)*. The proposed QCM scheme uses four LEDs (hence the name 'quad-LED'); while the magnitudes of the real and imaginary parts are conveyed through intensity modulation of LEDs, the sign information is conveyed through spatial indexing of LEDs. The proposed DCM scheme, on the other hand, exploits the polar representation of a complex symbol; it uses only two LEDs (hence the name 'dual-LED'), one LED to map the magnitude and another LED to map the phase of a complex modulation symbol. These techniques do not need Hermitian symmetry operation to generate LED compatible positive real transmit signals. We present zero-forcing and minimum distance detectors and their performance for QCM-OFDM and DCM-OFDM. We further propose another modulation scheme, termed as SM-DCM *(spatial modulation-DCM)* scheme, which brings in the advantage of spatial modulation (SM) to DCM. The proposed SM-DCM scheme uses two DCM BLOCKs with two LEDs in each BLOCK, and an index bit decides which among the two BLOCKs will be used in a given channel use. We study the bit error rate (BER) performance of the proposed schemes through analysis and simulations. Using tight analytical BER upper bounds and spatial distribution of the received signal-to-noise ratios, we compute and plot the achievable rate contours for a given target BER in QCM, DCM, and SM-DCM.

Keywords – *Visible light communication, quad-LED complex modulation (QCM), dual-LED complex modulation (DCM), QCM with phase rotation, SM-DCM, OFDM.*

I. INTRODUCTION

Wireless communication using visible light wavelengths (400 to 700 nm) in indoor local area network environments is emerging as a promising area of research [1]. Visible light communication (VLC) is evolving as an appealing complementary technology to radio frequency (RF) communication technology [2]. In VLC, simple and inexpensive light emitting diodes (LED) and photo diodes (PD) act as signal transmitters and receptors, respectively, replacing more complex and expensive transmit/receive RF hardware and antennas in RF wireless communication systems. Other favorable features in VLC include availability of abundant visible light spectrum at no cost, no licensing/RF radiation issues, and inherent security in closed-room applications. The possibility of using the same LEDs to simultaneously provide both energy-efficient lighting

as well as high-speed short-range communication is another attractive feature.

The potential to use multiple LEDs and PDs in multiple-input multiple-output (MIMO) array configurations has enthused MIMO wireless researchers to take special interest in VLC [3]-[9]. Signaling schemes considered in multiple-LED VLC include space shift keying (SSK) and its generalization (GSSK), where the ON/OFF status of the LEDs and the indices of the LEDs which are ON convey information bits [6],[7]. Other multiple-LED signaling schemes considered in the literature include spatial multiplexing (SMP), spatial modulation (SM), and generalized spatial modulation (GSM) [4],[8],[9],[10]. These works have considered real signal sets like M-ary pulse amplitude modulation (PAM) with positive-valued signal points in line with the need for the transmit signal in VLC to be positive and real-valued to intensity modulate the LEDs.

The VLC channel between an LED and a photo detector in indoor environments can be a multipath channel. The multipath effects can be mitigated by using orthogonal frequency division multiplexing (OFDM). The use of complex signal sets like M-ary quadrature amplitude modulation (QAM) along with OFDM in VLC is studied extensively in the literature [11]-[22]. Techniques reported in these works include DC-biased optical (DCO) OFDM [12], asymmetrically clipped optical (ACO) OFDM [16]-[17], flip OFDM [18],[19], non-DC biased (NDC) OFDM [21], and index modulation for NDC OFDM [22]. A key constraint in the above techniques, however, is that they perform Hermitian symmetry operation on the QAM symbol vector at the IFFT input so that the IFFT output would be positive and real-valued. A consequence of this is that N channel uses are needed to send $N/2$ symbols.

In this paper, we propose two simple and novel complex modulation techniques for VLC using multiple LEDs, which do not need Hermitian symmetry operation. The proposed schemes exploit the spatial dimension to convey complex-valued modulation symbols.

- The first proposed idea is to use four LEDs to form a single modulation unit that simultaneously conveys the real and imaginary parts of a complex modulation symbol and their sign information. While the magnitudes of the real and imaginary parts are conveyed through intensity modulation (IM) of LEDs, the sign information is conveyed through spatial indexing of LEDs. Since four LEDs form one complex modulation unit, we term this as *quad-LED complex modulation (QCM)* [23].
- The second idea is to exploit the representation of a com-

plex symbol in polar coordinates. Instead of conveying the real and imaginary parts of a complex symbol and their sign information using four LEDs in QCM, we can convey only the magnitude and phase of a complex symbol. We need only two LEDs for this purpose and there is no sign information to convey in this representation. So we use only two LEDs to form a single modulation unit in this case. We term this scheme as *dual-LED complex modulation (DCM)* since two LEDs constitute one complex modulator.

- The third proposed idea is to bring in the advantages of spatial modulation to the DCM scheme. Instead of using all the four LEDs to transmit one complex symbol (as in QCM), we choose two out of four LEDs to transmit the magnitude and phase of a complex symbol as in DCM scheme. Since we have to choose one pair of LEDs (one BLOCK) out of two and each pair will perform the same operation as in DCM scheme, we term this scheme as *spatial modulation-DCM (SM-DCM)* [24].

We investigate the bit error performance of the proposed QCM, DCM, and SM-DCM schemes[1] through analysis and simulations. We obtain upper bounds on the bit error rate (BER) of QCM, DCM, and SM-DCM. These analytical bounds are very tight at high signal-to-noise ratios (SNR). Therefore, these bounds enable us to easily compute and plot the achievable rate contours for a desired a target BER (e.g., 10^{-5} BER) in QCM, DCM, and SM-DCM. The analytical and simulation results show that the QCM, DCM, SM-DCM schemes achieve good BER performance. DCM has the advantage of fewer LEDs (2 LEDs) per complex modulator and better performance compared to QCM for small-sized modulation alphabets (e.g., 8-QAM). On the other hand, QCM has the advantage of additional degrees of freedom (4 LEDs) compared to DCM, because of which it achieves better performance compared to DCM for large alphabet sizes (e.g., 16-QAM, 32-QAM, 64-QAM). SM-DCM achieves better performance compared to DCM and QCM for small-sized modulation alphabets (e.g., 16-QAM) since it requires smaller modulation size. On the other hand, for large alphabet sizes, SM-DCM performs better compared to QCM at low E_b/N_0 values due to lower order modulation size, whereas at high E_b/N_0 values, SM-DCM performance degrades because of the reduced average relative distance between transmit vectors compared to QCM.

Since QCM and DCM can directly handle complex symbols in VLC, techniques which are applied to complex modulation schemes to improve performance in RF wireless channels can be applied to VLC as well. For example, it is known that rotation of complex modulation symbols can improve BER performance in RF wireless communication [25]. Motivated by this observation, we explore the possibility of achieving performance improvement in VLC through phase rotation of complex modulation symbols prior to mapping the signals to the LEDs in QCM. We term this scheme as QCM with phase rotation (QCM-PR). Results show that phase rotation of modulation symbols indeed can improve the BER perfor-

mance of QCM in VLC. We also study the proposed QCM and DCM schemes when used along with OFDM; we refer to these schemes as QCM-OFDM and DCM-OFDM. We present zero-forcing and minimum distance detectors and their performance for QCM-OFDM and DCM-OFDM.

The rest of this paper is organized as follows. The indoor VLC system model is presented in Section II. The proposed QCM, QCM-PR, and QCM-OFDM schemes and their performance are presented in Section III. Section IV presents the proposed DCM and DCM-OFDM schemes and their performance. Section V presents the proposed SM-DCM scheme and it performance. Section VI presents the spatial distribution of the received SNRs and the rate contours achieved in QCM, DCM, and SM-DCM. Conclusions are presented in Section VII.

II. INDOOR VLC SYSTEM MODEL

Consider an indoor VLC system with N_t LEDs (transmitter) and N_r photo detectors (receiver). Assume that the LEDs have a Lambertian radiation pattern [26],[27]. In a given channel use, each LED is either OFF or emits light with some intensity which is the magnitude of either the real part or imaginary part of a complex modulation symbol. An LED which is OFF implies a light intensity of zero. Let $\mathbf{x} = [x_1 \ x_2 \ \cdots x_{N_t}]^T$ denote the $N_t \times 1$ transmit signal vector, where x_i is the light intensity emitted by the ith LED. Let $\mathbf{H}$ denote the $N_r \times N_t$ MIMO VLC channel matrix:

$$\mathbf{H} = \begin{bmatrix} h_{11} & h_{12} & h_{13} & \cdots & h_{1N_t} \\ h_{21} & h_{22} & h_{23} & \cdots & h_{2N_t} \\ \vdots & \vdots & \ddots & \vdots & \vdots \\ h_{N_r1} & h_{N_r2} & h_{N_r3} & \cdots & h_{N_rN_t} \end{bmatrix}, \quad (1)$$

where h_{ij} is the channel gain between jth LED and ith photo detector, $j = 1, 2, \cdots, N_t$ and $i = 1, 2, \cdots, N_r$. As in [4], we consider only the line-of-sight (LOS) paths between the LEDs and the photo detectors. From [26], the LOS channel gain h_{ij} is calculated as (see Fig. 1 for the definition of various angles in the model)

$$h_{ij} = \frac{n+1}{2\pi} \cos^n \phi_{ij} \, \cos \theta_{ij} \frac{A}{R_{ij}^2} \mathrm{rect}\Big(\frac{\theta_{ij}}{FOV}\Big), \quad (2)$$

where ϕ_{ij} is the angle of emergence with respect to the jth source (LED) and the normal at the source, n is the mode number of the radiating lobe given by $n = \frac{-\ln(2)}{\ln \cos \Phi_{\frac{1}{2}}}$, $\Phi_{\frac{1}{2}}$ is the half-power semiangle of the LED [27], θ_{ij} is the angle of incidence at the ith photo detector, A is the area of the detector, R_{ij} is the distance between the jth source and the ith detector, FOV is the field of view of the detector, and $\mathrm{rect}(x) = 1$, if $|x| \leq 1$, and $\mathrm{rect}(x) = 0$, if $|x| > 1$.

The LEDs and the photo detectors are placed in a room of size 5m×5m×3.5m as shown in Fig. 1. The LEDs are placed at a height of 0.5m below the ceiling and the photo detectors are placed on a table of height 0.8m. Let d_{tx} denote the distance between the LEDs and d_{rx} denote the distance between the photo detectors.

Assuming perfect synchronization, the $N_r \times 1$ received signal vector at the receiver is given by

$$\mathbf{y} = a\mathbf{H}\mathbf{x} + \mathbf{n}, \quad (3)$$

[1]We note that in all the three schemes, the number of LEDs that will be simultaneously ON in a channel use is two.
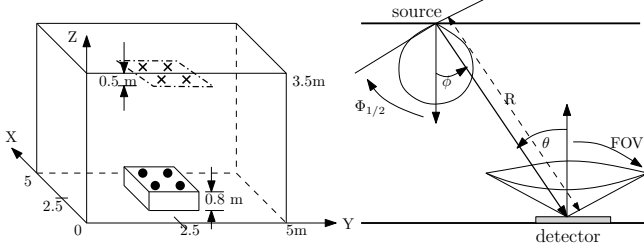
Fig. 1. Geometric set-up of the considered indoor VLC system. A dot represents a photo detector and a cross represents an LED.

where a is the responsivity of the detector [28] and $\mathbf{n}$ is the noise vector of dimension $N_r \times 1$. Each element in the noise vector $\mathbf{n}$ is the sum of received thermal noise and ambient shot light noise, which can be modeled as i.i.d. real AWGN with zero mean and variance σ^2 [29]. The average received signal-to-noise ratio (SNR) is given by $\overline{\gamma} = \frac{a^2 P_r^2}{\sigma^2}$, where $P_r^2 = \frac{1}{N_r} \sum_{i=1}^{N_r} \mathbb{E}[|\mathbf{H}_i \mathbf{x}|^2]$, and $\mathbf{H}_i$ is the ith row of $\mathbf{H}$.

III. PROPOSED QCM SCHEME

A. QCM transmitter

The proposed QCM scheme uses four LEDs at the transmitter. Figure 2 shows the block diagram of a QCM transmitter. Let $\mathbb{A}$ denote the complex modulation alphabet used (e.g., QAM). In each channel use, one complex symbol from $\mathbb{A}$ (chosen based on $\log_2 |\mathbb{A}|$ information bits) is signaled by the four LEDs as described below.

Each complex modulation symbol can have a positive or negative real part, and a positive or negative imaginary part. For example, the signal set for 16-QAM is $\{\pm1 \pm j1, \pm1 \pm j3, \pm3 \pm j1, \pm3 \pm j3\}$. Let $s \in \mathbb{A}$ be the complex symbol to be signaled in a given channel use. Let

$$s = s_I + j s_Q,$$

where s_I and s_Q are the real and imaginary parts of s, respectively. Two LEDs (say, LED1 and LED2) are used to convey the magnitude and sign of s_I as follows. LED1 will emit with intensity $|s_I|$ if s_I is positive (≥ 0), whereas LED2 will emit with the same intensity $|s_I|$ if s_I is negative (< 0). Note that, since s_I is either ≥ 0 or < 0, only any one of LED1 and LED2 will be ON in a given channel use and the other will be OFF. In a similar way, the remaining two LEDs (i.e., LED3 and LED4) will convey the magnitude and sign of s_Q in such a way that LED3 will emit intensity $|s_Q|$ if s_Q is ≥ 0, whereas LED4 will emit with the same intensity $|s_Q|$ if s_Q is < 0. Therefore, QCM sends one complex symbol in one channel use. The mapping of the magnitudes and signs of s_I and s_Q to the activity of LEDs in a given channel use is summarized in Table I.

Example 1: If $s = -3 + j1$, then the LEDs will be activated as follows: LED1: OFF; LED2: emits 3; LED3: emits 1; LED4: OFF. The $N_t \times 1$ (i.e., 4×1) QCM transmit vector in this example is $\mathbf{x} = [0\ 3\ 1\ 0]^T$. Likewise, if $s = 1 - j3$, then activation of LEDs will be as follows: LED1: emits 1; LED2: OFF; LED3: OFF; LED4: emits 3. The corresponding QCM transmit vector is $\mathbf{x} = [1\ 0\ 0\ 3]^T$.
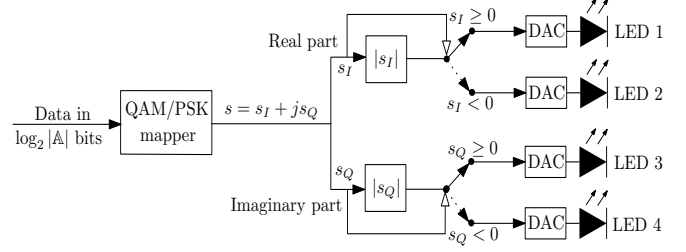

Fig. 2. QCM transmitter.

Real part s_I	Status of LEDs	Imag. part s_Q	Status of LEDs
≥ 0	LED1 emits $|s_I|$ LED2 is OFF	≥ 0	LED3 emits $|s_Q|$ LED4 is OFF
< 0	LED1 is OFF LED2 emits $|s_I|$	< 0	LED3 is OFF LED4 emits $|s_Q|$

TABLE I
MAPPING OF COMPLEX SYMBOL s (WITH REAL PART s_I AND IMAGINARY PART s_Q) TO LEDs ACTIVITY IN QCM.

Remark 1: Because of the proposed mapping, in any given channel use, two LEDs (one among LED1 and LED2, and another one among LED3 and LED4) will be ON simultaneously and the remaining two LEDs will be OFF.

Remark 2: The complex symbol conveyed in a channel use can be detected from the received QCM signal using the knowledge of the QCM map (Table I) at the receiver.

B. QCM signal detection

Figure 3 shows the block diagram of a QCM receiver with $N_r = 4$ PDs. Following the system model in Sec. II, the $N_r \times 1$ received signal vector at the output of the PDs is given by (3). Assuming perfect channel knowledge at the receiver, the maximum likelihood (ML) estimate of the transmit vector $\mathbf{x}$ is obtained as

$$\hat{\mathbf{x}}_{ML} = \underset{\mathbf{x} \in \mathbb{S}_Q}{\operatorname{argmin}} \|\mathbf{y} - a\mathbf{H}\mathbf{x}\|^2, \tag{4}$$

where $\mathbb{S}_Q$ denotes the QCM signal set (consisting of all possible $\mathbf{x}$ vectors). The detected vector $\hat{\mathbf{x}}_{ML}$ is demapped to the corresponding complex symbol $\hat{s}_{ML}$, which is then demapped to get the corresponding information bits.

C. BER performance of QCM

In this subsection, we present the BER performance of QCM obtained through an analytical upper bound on the BER and simulations.

1) Upper bound on BER: Consider the QCM system model in (3). Normalizing the elements of the noise vector to unit variance, the received vector can be written as

$$\mathbf{y} = \frac{a}{\sigma}\mathbf{H}\mathbf{x} + \mathbf{n}. \tag{5}$$

The ML detection rule for QCM can be rewritten as

$$\hat{\mathbf{x}}_{ML} = \underset{\mathbf{x}}{\operatorname{argmin}} \left(\frac{a}{\sigma}\|\mathbf{H}\mathbf{x}\|^2 - 2\mathbf{y}^T\mathbf{H}\mathbf{x} \right). \tag{6}$$

Assuming that the channel matrix $\mathbf{H}$ is known at the receiver, the pairwise error probability (PEP) – probability that the
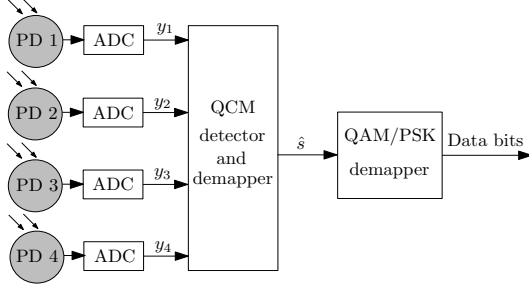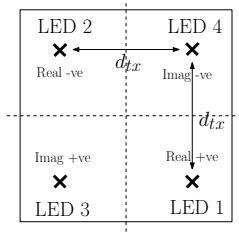
Fig. 3. QCM receiver.

Fig. 4. Placement of LEDs and signal mapping to LEDs.

Room	Length (X)	5m
	Width (Y)	5m
	Height (Z)	3.5m
Transmitter	No. of LEDs (N_t)	4
	Height from the floor	3m
	Elevation	$-90°$
	Azimuth	$0°$
	$\Phi_{1/2}$	$60°$
	Mode number, n	1
	d_{tx}	0.2m to 4.8m
Receiver	No. of PDs (N_r)	4
	Height from the floor	0.8m
	Elevation	$90°$
	Azimuth	$0°$
	Responsivity, a	1 Ampere/Watt
	FOV	$85°$
	d_{rx}	0.1m

TABLE II
SYSTEM PARAMETERS IN THE CONSIDERED INDOOR VLC SYSTEM.

receiver decides in favor of the signal vector $\mathbf{x}_2$ when $\mathbf{x}_1$ was transmitted – can be written as

$$
\begin{aligned}
PEP(\mathbf{x}_1 \to \mathbf{x}_2|\mathbf{H}) &= \Pr(\mathbf{x}_1 \to \mathbf{x}_2|\mathbf{H}) \\
&= \Pr\left(\mathbf{y}^T\mathbf{H}(\mathbf{x}_2 - \mathbf{x}_1) > \frac{a}{2\sigma}\big(\|\mathbf{H}\mathbf{x}_2\|^2 - \|\mathbf{H}\mathbf{x}_1\|^2\big) \right) \\
&= \Pr\left(\frac{2\sigma}{a}\mathbf{n}^T\mathbf{H}(\mathbf{x}_2 - \mathbf{x}_1) > \|\mathbf{H}(\mathbf{x}_2 - \mathbf{x}_1)\|^2 \right).
\end{aligned} \tag{7}
$$

Define $z \triangleq \frac{2\sigma}{a}\mathbf{n}^T\mathbf{H}(\mathbf{x}_2 - \mathbf{x}_1)$. We can see that z is a Gaussian random variable with mean $\mathbb{E}(z) = 0$ and variance $\mathrm{Var}(z) = \frac{4\sigma^2}{a^2}\|\mathbf{H}(\mathbf{x}_2 - \mathbf{x}_1)\|^2$. Therefore, (7) can be written as

$$
PEP(\mathbf{x}_1 \to \mathbf{x}_2|\mathbf{H}) = Q\left(\frac{a}{2\sigma}\|\mathbf{H}(\mathbf{x}_2 - \mathbf{x}_1)\| \right). \tag{8}
$$

Let $\eta = \log_2 M$ bpcu and $L \triangleq |\mathbb{S}_Q|$. An upper bound on the QCM BER for ML detection can be obtained using union bound as

$$
\begin{aligned}
BER &\leq \frac{1}{L} \sum_{i=1}^{L} \sum_{j=1, i\neq j}^{L-1} PEP(\mathbf{x}_i \to \mathbf{x}_j|\mathbf{H}) \frac{d_H(\mathbf{x}_i, \mathbf{x}_j)}{\eta} \\
&= \frac{1}{L} \sum_{i=1}^{L} \sum_{j=1, i\neq j}^{L-1} Q\left(\frac{a}{2\sigma}\|\mathbf{H}(\mathbf{x}_j - \mathbf{x}_i)\| \right) \frac{d_H(\mathbf{x}_i, \mathbf{x}_j)}{\eta},
\end{aligned} \tag{9}
$$

where $d_H(\mathbf{x}_i, \mathbf{x}_j)$ is the Hamming distance between the bit mappings corresponding to the signal vectors $\mathbf{x}_i$ and $\mathbf{x}_j$.

2) Results and discussions: We evaluated the BER performance of QCM through the analytical upper bound and simulations. The various system parameters used in the performance evaluation are listed in Table II. The placement of LEDs and the signal mapping to these LEDs used are shown Fig. 4. We evaluate the performance of QCM for various modulation alphabets including BPSK, 4-, 16-, and 64-QAM.

In Fig. 5, we plot the analytical upper bound and the simulated BER for QCM with $d_{tx} = 1$m, 4-QAM, 16-QAM, $N_r = 4$, and ML detection. It can be seen that the analytical upper bound on the BER of QCM is very tight at moderate

to high SNRs. In Fig. 6, we plot the simulated BER of QCM with $d_{tx} = 1$m and ML detection for BPSK (1 bpcu), 4-QAM (2 bpcu), 16-QAM (4 bpcu), and 64-QAM (6 bpcu). From Fig. 6, we observe that QCM achieves 10^{-4} BER at an E_b/N_0 of about 37 dB for BPSK, 40 dB for 4-QAM, 42.5 dB for 16-QAM, and 46.5 dB for 64-QAM. This observed increase in the required E_b/N_0 for increased QAM size is because of the reduced minimum distance for larger QAM size, and it is in line with what happens in conventional RF modulation. In addition, we observe crossovers which show better performance for larger-sized QAM at low SNRs (e.g., crossover between the performance of 4-QAM and 16-QAM at around 4×10^{-2} BER). This crossover occurs due to the degrading effect of an equal-power interferer[2] on the one hand, and the benefit of a strong interferer in multiuser detection[3] on the other hand. This can be further explained with the following example. The signal received at the ith PD is $y_i = h_l|s_I| + h_k|s_Q| + n_i$, where h_l and h_k are the channel gains corresponding to the LEDs chosen to transmit $|s_I|$ and $|s_Q|$, respectively. For 4-QAM, the transmit signals from both the active LEDs will be 1 (i.e., both $|s_I|$ and $|s_Q|$ will be 1). Whereas for 16-QAM, the transmit signal from each active LED can be 1 or 3 (i.e., $|s_I|$ can be 1 or 3, and so is $|s_Q|$). Therefore, the received signal for 4-QAM is $y_i = h_l + h_k + n_i$. Also, h_l and h_k can be nearly equal because of high channel correlation, making 4-QAM detection unreliable at low SNRs. Whereas, since $|s_I|, |s_Q| \in \{1, 3\}$ in 16-QAM, the effect of channel correlation between h_l and h_k in 16-QAM detection is reduced. That is, $\mathbb{E}\big(|h_l|s_I| - h_k|s_Q||\big)$ is larger for 16-QAM compared to that for 4-QAM.

Effect of varying d_{tx}: Figure 7 shows the effect of varying the spacing between the LEDs (d_{tx} varied in the range 0.2m to 4.8m) on the BER performance of QCM with 4-QAM and 16-QAM at $E_b/N_0 = 35$ dB. From Fig. 7, we see that there is an optimum d_{tx} (around 3m) which gives the best BER performance. If d_{tx} is increased above and decreased below this optimum spacing, the BER worsens. The reason for this optimum can be explained as follows. On the one hand, the

---

[2]Signals from two active LEDs interfere with each other at the receiver.
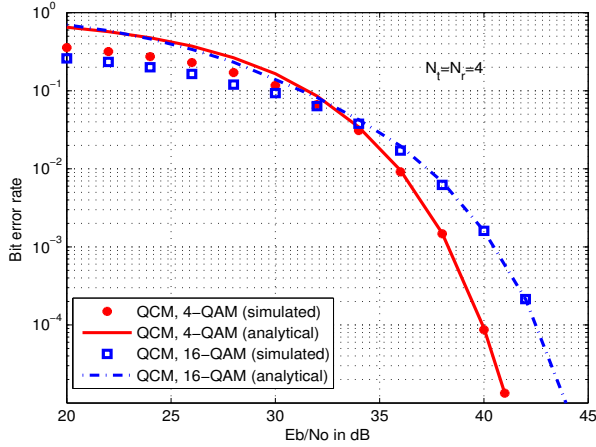[3]A strong interferer can be effectively canceled in a multiuser detector [30].

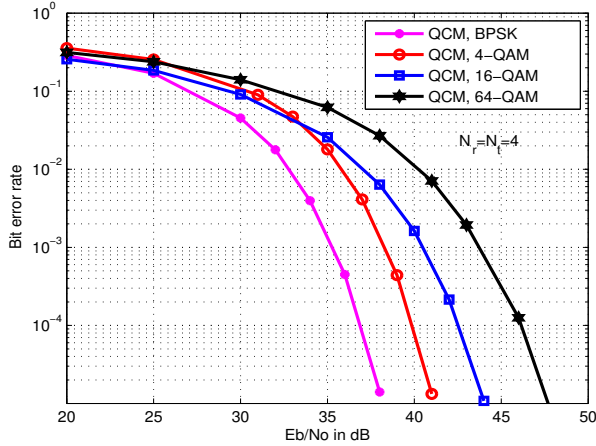Fig. 5. Comparison of analytical upper bound and simulated BER for QCM with $d_{tx} = 1$m, 4-QAM, and 16-QAM.

Fig. 6. BER performance of QCM with BPSK, 4-QAM, 16-QAM, and 64-QAM at $d_{tx} = 1$m.

channel gains get weaker as d_{tx} is increased. This reduces the received signal level, which is a source of BER degradation. On the other hand, the channel correlation also gets weaker as d_{tx} is increased. This reduced channel correlation is a source of BER improvement. These opposing effects of weak channel gains and weak channel correlations for increasing d_{tx} results in an optimum spacing. Also, as observed and explained in Fig. 6, in Fig. 7 also we see that QCM with 16-QAM can perform a little better than QCM with 4-QAM when d_{tx} is small and channel correlation is high.

D. QCM with phase rotation

As we mentioned earlier, rotation of complex modulation symbols is known to improve BER performance in RF communications [25]. Motivated by this and the fact that QCM allows the use of complex modulation alphabets in VLC, in this subsection we study the performance QCM scheme with rotation of the complex modulation symbols.

1) QCM-PR transmitter: In QCM with phase rotation, a complex symbol from a modulation alphabet $\mathbb{A}$ is rotated by a phase angle of θ before being transmitted by the quad-LED setup. Let $s \in \mathbb{A}$ be the complex symbol chosen based on the input information bits. Instead of sending the symbol s as such in QCM, the QCM-PR transmitter sends the rotated
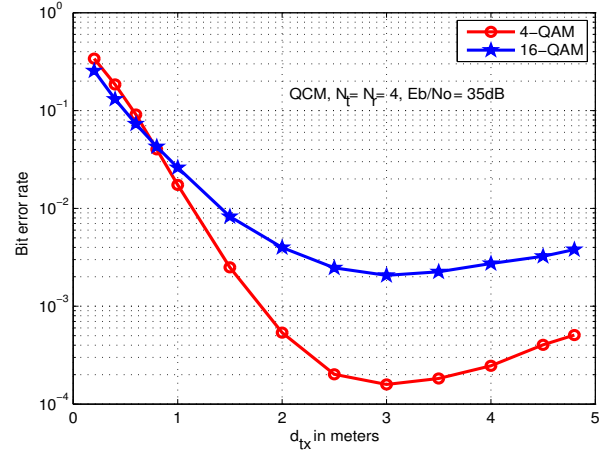

Fig. 7. BER performance of QCM as a function of d_{tx} for 4-QAM and 16-QAM at $E_b/N_0 = 35$ dB.

complex symbol s' given by

$$s' = e^{j\theta}s \tag{10}$$

through the quad-LED setup as described before. Therefore,

$$
\begin{aligned}
s'_I &= s_I \cos\theta - s_Q \sin\theta, \\
s'_Q &= s_I \sin\theta + s_Q \cos\theta.
\end{aligned} \tag{11}
$$

Let $\mathbf{x}'$ be the QCM transmit vector constructed using s'_I and s'_Q. Now, $\mathbf{x}'$ is the transmitted vector corresponding to the complex signal s rotated by a phase angle θ.

2) QCM-PR signal detection: We assume that the angle of rotation θ is known both at the transmitter and receiver. The ML estimate of the transmitted symbol s is then given by

$$\hat{\mathbf{x}}'_{ML} = \underset{\mathbf{x}' \in \mathbb{S}_{QP}}{\arg\min} \|\mathbf{y} - a\mathbf{H}\mathbf{x}'\|^2. \tag{12}$$

where $\mathbb{S}_{QP}$ denotes the QCM-PR signal set. The detected vector $\hat{\mathbf{x}}'_{ML}$ is demapped to the corresponding complex symbol $\hat{s}'_{ML}$, which is then demapped to get the corresponding information bits.

3) BER performance of QCM-PR: We evaluated the BER performance of QCM-PR scheme. The simulation parameter settings, LEDs placement, and signal mapping to LEDs are same as those used in Sec. III-C.

BER as a function of rotation angle θ: In Fig. 8, we plot the BER of QCM-PR scheme as a function of the rotation angle θ (in degrees) at $d_{tx} = 1$m. BER plots for 4-QAM with $E_b/N_0 = 37$ dB and 16-QAM with $E_b/N_0 = 40$ dB are shown. We limit the range of θ value in the x-axis from $0°$ to $90°$ as the pattern of the plots repeat after $90°$ due to symmetry. Note that $\theta = 0°$ corresponds to the basic QCM without rotation. The following interesting observations can be made from Fig. 8. First, for both 4-QAM and 16-QAM, the BER plots are symmetrical with respect to $45°$, which can be expected. Second, for 4-QAM, $\theta = 45°$ happens to be the
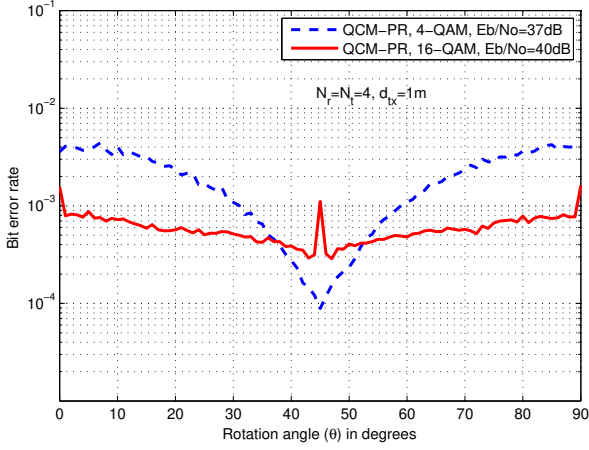
Fig. 8. BER performance of QCM-PR as a function of rotation angle θ for 4-QAM, $E_b/N_0 = 37$ dB and 16-QAM, $E_b/N_0 = 40$ dB at $d_{tx} = 1$m.

Fig. 9. BER versus E_b/N_0 characteristics of QCM and QCM-PR for 4-QAM and 16-QAM at $d_{tx} = 1$m.

optimum rotation which gives the best BER[4]. Note that there is more than an order improvement in BER at this optimum rotation compared to basic QCM without rotation (see BERs at $\theta = 0°$ and $\theta = 45°$). Third, for 16-QAM, there are two optimum angles around $45°$ because of symmetry; $\theta = 43°$ is one of them. Figure 9 shows a comparison between the BER performance of QCM-PR (with optimum rotation angles) and QCM (no rotation) at $d_{tx} = 1$m. BER plots for 4-QAM and 16-QAM are shown. It can be seen that optimum phase rotation improves the BER performance by about 2 to 3 dB.

QCM-PR vs QCM for different d_{tx}: Figure 10 shows how varying d_{tx} affects the BER performance of QCM-PR and QCM at $E_b/N_0 = 35$ dB. As observed for QCM in Fig. 7, we see that there is an optimum spacing in QCM-PR as well, which is due to the opposing effects of weak channel gains and weak channel correlation for increasing d_{tx} values. QCM-PR achieves better performance compared to QCM. For example, at $d_{tx} = 3$m, there is about 3 orders of BER improvement for 4-QAM. This reinforces the benefit of phase rotation.

E. QCM-OFDM

Since QCM allows the transmission of complex symbols using the quad-LED setup, OFDM signaling can be carried out using QCM. In this subsection, we present the QCM-OFDM scheme, its detection, and performance.

1) QCM-OFDM transmitter: In the QCM-OFDM transmitter, N complex symbols from $\mathbb{A}$ (chosen based on $N \log_2 |\mathbb{A}|$ information bits) will be transmitted by the four LEDs in N channel uses, where N is the number of subcarriers. The N complex symbols $\mathbf{v} = [v_1, v_2, \cdots, v_N]^T \in \mathbb{A}^N$ are transformed using inverse Fourier transform (IFFT) to obtain the complex transmit symbols $\mathbf{s} = [s_1, s_2, \cdots, s_N]^T = \mathbf{F}^H \mathbf{v}$, where $\mathbf{F}$ is the Fourier transform matrix. The N output symbols from the IFFT block are then transmitted one by

---

Fig. 10. BER versus LED spacing (d_{tx}) characteristics of QCM and QCM-PR for 4-QAM and 16-QAM at $E_b/N_0 = 35$ dB.

one in N channel uses by the quad-LED setup in the QCM transmitter. Thus, effectively N complex modulation symbols are sent in N channel uses. Let $\mathbf{x}_n$ denote the $N_t \times 1$ (i.e., 4×1) transmit vector corresponding to s_n, $n = 1, 2, \cdots, N$.

2) QCM-OFDM signal detection: Let $\mathbf{Y} = [\mathbf{y}_1, \mathbf{y}_2, \cdots, \mathbf{y}_N]$ be the matrix of received vectors corresponding to the matrix of transmit vectors $\mathbf{X} = [\mathbf{x}_1, \mathbf{x}_2, \cdots, \mathbf{x}_N]$, i.e., corresponding to the signal vector $\mathbf{s} = [s_1, s_2, \cdots, s_N]^T$. Before performing Fourier transform (FFT) operation, we need to detect the transmitted symbols $s_i \in [0, \infty)$. This detection involves two stages, namely, (i) active LEDs identification, and (ii) complex symbol reconstruction.

Active LEDs identification: To discern the two active LEDs in the quad-LED setup, we compute

$$z_{i,j} = (\mathbf{h}_j^T \mathbf{h}_j)^{-1} \mathbf{h}_j^T \mathbf{y}_i, \quad j = 1, 2, 3, 4, \quad i = 1, \cdots, N, \quad (13)$$

where $\mathbf{h}_j$ is the jth column of the channel matrix $\mathbf{H}$. For the ith channel use, the LEDs corresponding to the two largest values of $|z_{i,j}|$ are detected to be active. That is, if i_1 and i_2

---

[4]It is interesting to note that QCM-PR with 4-QAM and $\theta = 45°$ rotation specializes to SSK with $N_t = 4$. That is, the 4-QAM signal set when rotated by $45°$ becomes $\{1 + j0, 0 + j1, -1 + j0, 0 - j1\}$ When mapped to the LEDs as per QCM, the resulting QCM signal set becomes $\{[1000]^T, [0010]^T, [0100]^T, [0001]^T\}$, which is the same as the SSK signal set with $N_t = 4$. Because of this, only one LED will be ON at a time in QCM-PR with $\theta = 45°$ and therefore there will be no interference.
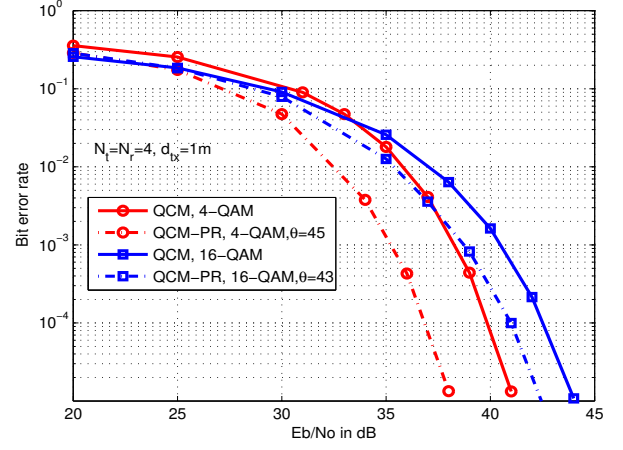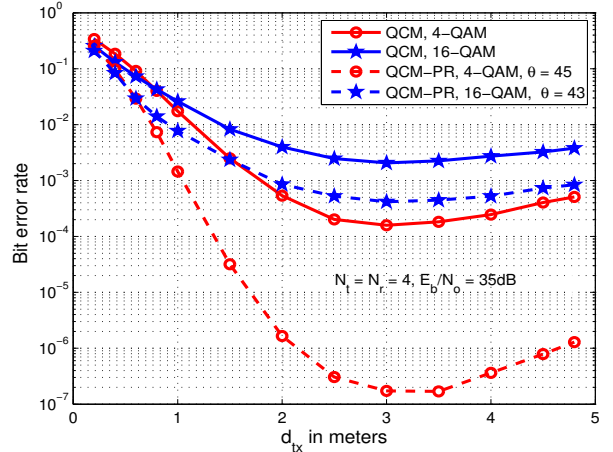
are the indices of the active LEDs in the ith channel use, then

$$\hat{i}_1 = \underset{j \in \{1,2,3,4\}}{\text{argmax}} |z_{i,j}| \qquad i_1 \in \{1,2,3,4\}$$

$$\hat{i}_2 = \underset{j \in \{1,2,3,4\} \setminus i_1}{\text{argmax}} |z_{i,j}| \qquad i_2 \in \{1,2,3,4\} \setminus i_1.$$

Complex symbol reconstruction: After identifying the active LEDs, we need to detect s_I and s_Q. This can be achieved through a zero-forcing (ZF) type detector. Let $\mathbf{s}_i = [s_I^i, s_Q^i]^T$ be the transmitted signal values corresponding to the complex signal s_i. Form $\mathbf{H}_{ZF}$ matrix using the i_1th and i_2th columns of $\mathbf{H}$ as $\mathbf{H}_{ZF} = [\mathbf{h}_{i_1} \ \mathbf{h}_{i_2}]$. Now, the ZF detector output is given by

$$\hat{\mathbf{s}}_i = \frac{1}{r}(\mathbf{H}_{ZF}^T \mathbf{H}_{ZF})^{-1}\mathbf{H}_{ZF}^T \mathbf{y}_i. \tag{14}$$

Finally, an estimate of the transmitted complex symbol is obtained as $\hat{s}_i = \hat{s}_I^i + \mathrm{j}\hat{s}_Q^i$. Now, $\hat{\mathbf{v}} = \mathbf{F}\hat{\mathbf{s}}$. The $N \log_2 |\mathbb{A}|$ information bits are demapped from $\hat{\mathbf{v}}$.

3) Minimum distance detector: The above zero forcing detector is a sub-optimal detector. Therefore, to further improve the performance of QCM-OFDM, we use a minimum distance (MD) detector. This detector is described as follows. Let $\mathbb{S}_F$ be the set of all possible values the vector $\mathbf{s}$ can take, i.e., $\mathbf{s} \in \mathbb{S}_F$ and $|\mathbb{S}_F| = |\mathbb{A}^N|$. $\mathbf{x}_n$ is the QCM transmit vector in the nth channel use, $n = 1, 2, \cdots, N$, and $\mathbf{X} = [\mathbf{x}_1, \mathbf{x}_2, \cdots, \mathbf{x}_N]$ is the matrix of QCM transmit vectors for one QCM-OFDM symbol. Let $\mathbb{S}_{QO}$ be the set of all possible values of the matrix $\mathbf{X}$, i.e., $\mathbf{X} \in \mathbb{S}_{QO}$ and $|\mathbb{S}_{QO}| = |\mathbb{A}^N|$. Therefore, for every $\mathbf{v} \in \mathbb{A}$ there exists a corresponding matrix $\mathbf{X} \in \mathbb{S}_{QO}$ and vice versa. The estimate of $\mathbf{v}$ in the MD detector is obtained as

$$\hat{\mathbf{v}} = \underset{\mathbf{X} \in \mathbb{S}_{QO}}{\text{argmin}} \|\mathbf{Y} - a\mathbf{H}\mathbf{X}\|. \tag{15}$$

The $N \log_2 |\mathbb{A}|$ information bits are demapped from $\hat{\mathbf{v}}$.

4) BER performance of QCM-OFDM: We evaluated the BER performance of QCM-OFDM scheme. The simulation parameter settings, LEDs placement, and signal mapping to LEDs are same as those used in Sec. III-C. Figure 11 shows the BER performance of QCM-OFDM with $N = 8$ and 4-QAM at $d_{tx} = 1$m. The performance achieved by ZF detection and MD detection (presented in the previous subsection) are plotted. It can be seen that the MD detector achieves better performance by 2.5 dB to 3.5 dB compared to the ZF detector. In Fig. 12, we compare the performance of QCM, QCM-PR with optimum rotation $\theta = 45°$, and QCM-OFDM with 4-QAM and $d_{tx} = 1$m. It can be seen that QCM-OFDM with MD detection achieves better performance compared to both QAM and QCM-PR. For example, at a BER of 10^{-4}, QCM-OFDM performs better than QCM-PR and QCM by about 2 dB and 5 dB, respectively.

IV. PROPOSED DCM SCHEME

The QCM scheme proposed in the previous section conveys the real and imaginary parts of a complex symbol and their sign information using four LEDs. Representation of complex symbols in polar coordinates can be exploited instead. That is, it is adequate to convey only the magnitude and phase (r, ϕ) of a complex symbol, for which only two LEDs suffice and there
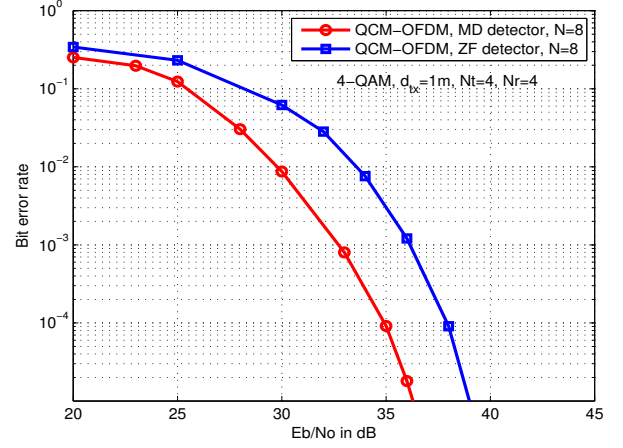

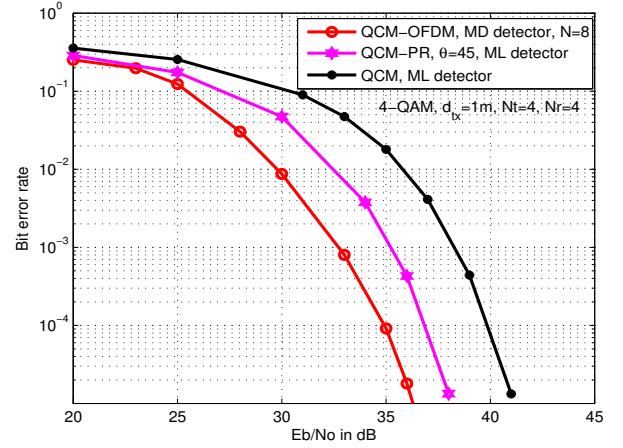Fig. 11. BER performance of QCM-OFDM with ZF detection and MD detection for $N = 8$, 4-QAM, $d_{tx} = 1$m.

Fig. 12. BER performance comparison between QCM, QCM-PR, and QCM-OFDM for 4-QAM at $d_{tx} = 1m$.

is no sign information to convey. The DCM scheme proposed in this section is based on this idea. The proposed DCM scheme uses two LEDs to convey the magnitude and phase of a complex symbol. The block diagram of DCM transmitter is given in Fig. 13. The complex modulation symbol s that is to be transmitted in a given channel use is split in to two real and non-negative parts, namely, the magnitude of the complex symbol r and the phase of the complex symbol ϕ such that

$$s = re^{j\phi},$$
$$r = |s|, \quad r \in \mathbb{R}^+,$$
$$\phi = \arg(s), \quad \phi \in [0, 2\pi). \tag{16}$$

Now, we use LED1 to transmit r and LED2 to transmit ϕ through intensity modulation. The 2×1 DCM transmit vector $\mathbf{x}$ is then given by $\mathbf{x} = [r \quad \phi]^T$.

Example 2: If the complex modulation symbol to be transmitted is $s = 3 + \mathrm{j}3$, then $r = 3\sqrt{2}$ and $\phi = \frac{\pi}{4}$. LED1 emits light of intensity $3\sqrt{2}$ and LED2 emits light of intensity $\frac{\pi}{4}$.

Remark 3: Note that in case of M-PSK modulation only the phases of the symbols convey information (because of constant magnitude). So the 'magnitude-LED' (LED1) in DCM essentially becomes redundant, and only the angle value sent on the 'angle-LED' (LED2) matters. Therefore, in this
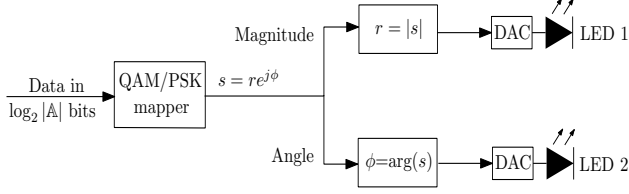
Fig. 13. DCM transmitter.

case, the DCM scheme can be viewed as equivalent to a single-LED scheme with M-PAM. However, in cases where M-PSK symbols undergo some pre-processing operation before transmission (e.g., IFFT operation on M-PSK symbols in OFDM), both the magnitude and angle of the resulting complex variables sent by LEDs 1 and 2 matter.

Now, the $N_r \times 1$ received signal vector at the receiver is given by

$$\mathbf{y} = a\mathbf{H}\mathbf{x} + \mathbf{n}, \quad (17)$$

and the ML estimate of the transmit vector $\mathbf{x}$ is given by

$$\hat{\mathbf{x}}_{ML} = \underset{\mathbf{x} \in \mathbb{S}_D}{\operatorname{argmin}} \|\mathbf{y} - a\mathbf{H}\mathbf{x}\|^2, \quad (18)$$

where $\mathbb{S}_D$ denotes the DCM signal set (consisting of all possible transmit vectors $\mathbf{x}$). The detected vector $\hat{\mathbf{x}}_{ML}$ is demapped to the corresponding complex symbol $\hat{s}_{ML}$, which is then demapped to get the corresponding information bits.

A. BER performance of DCM

An upper bound on the BER of QCM for ML detection was obtained in Sec. III-C1. In a similar way, an upper bound on the BER of DCM can be obtained. Figure 14 shows the upper bound and simulated BER plots for DCM with 8-QAM and 16-QAM. The system parameters used are the same as in Table II. The two LEDs are placed at the locations of LED1 and LED2 specified in Fig. 4, and $d_{tx} = 1$m. It can be seen that the upper bound is tight at moderate to high SNRs.

Figure 15 presents a BER vs E_b/N_0 performance comparison between DCM and QCM for 8-QAM, 16-QAM, and 64-QAM using ML detection. Table III also presents a similar performance comparison between DCM, QCM, and QCM-PR. In this Table, we present the E_b/N_0 (in dB) required to achieve a BER of 10^{-3} in DCM, QCM, and QCM-PR[5] for 8-, 16-, 32-, 64-QAM. From Fig. 15, we observe that DCM achieves better performance compared to QCM for a small-sized alphabet like 8-QAM; e.g., at a BER of 10^{-4}, DCM performs better than QCM by about 10.4 dB for 8-QAM. On the other hand, for larger-sized alphabets like 16-QAM and 64-QAM, QCM outperforms DCM by about 1 dB and 5 dB, respectively, at 10^{-4} BER. Similar observations can be made in Table III; DCM requires a lesser E_b/N_0 to achieve 10^{-3} BER compared to QCM for 8-QAM, whereas QCM requires less E_b/N_0 compared to DCM for 16-QAM, 32-QAM, and 64-QAM. This is because, for large QAM sizes, the average

[5]Note that, unlike in QCM, phase rotation in DCM essentially gives the same performance as DCM without phase rotation. This is because i) the magnitude of the complex number does not change on rotation, and hence the values of r transmitted by LED1 in DCM remain unaffected by rotation, and ii) the relative distance between the intensity levels transmitted for the phase information ϕ by LED2 in DCM does not change on rotation.
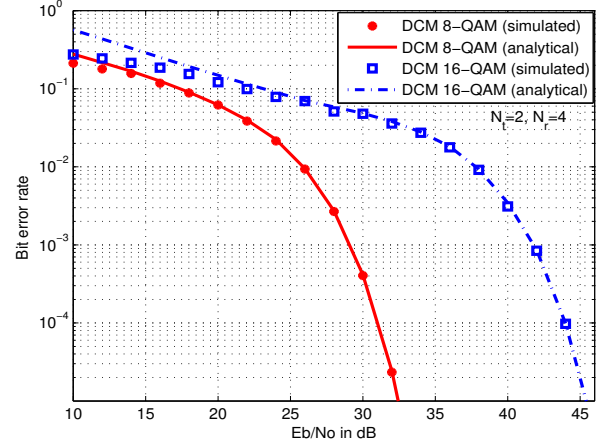

Fig. 14. Comparison of analytical upper bound and simulated BER for DCM with 8-QAM and 16-QAM.
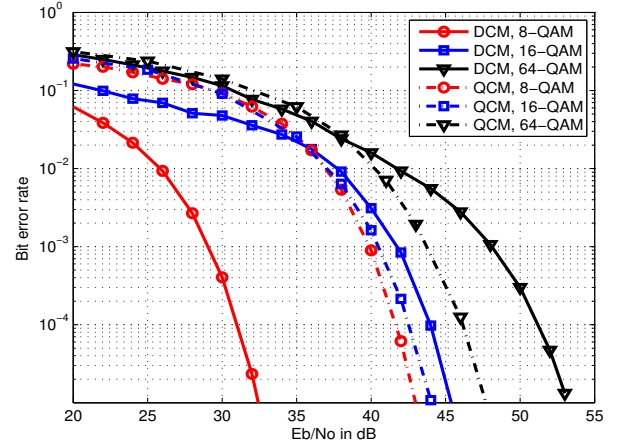

Fig. 15. Comparison of the BER performance of DCM and QCM for 8-QAM, 16-QAM, and 64-QAM.

relative distance between the transmit vectors in QCM is more compared to that in DCM, i.e., if $(\mathbf{x}_1, \mathbf{x}_2)$ is a pair of vectors from the transmit signal set, then $\mathbb{E}[\|\mathbf{x}_1 - \mathbf{x}_2\|]$ is larger for the QCM signal set than for the DCM signal set. For example, the intensities emitted in QCM for 16-QAM could be one of $\{0, 1, 3\}$. Whereas, the intensities emitted in DCM for 16-QAM could be one among the 3 different possible values for r and one among the 12 different possible values for ϕ. As the size of the modulation alphabet $\mathbb{A}$ increases, the set of possible values of r and ϕ increases as $O(|\mathbb{A}|)$ in DCM. Whereas, in QCM, as the size of the modulation alphabet increases, the cardinality of the set of possible transmit intensity levels is only $\sqrt{|\mathbb{A}|}/2 + 1$ if $\mathbb{A}$ is square QAM, and $\sqrt{|\mathbb{A}/2|} + 1$ if $\mathbb{A}$ is non-square.

Spectral efficiency in bpcu	DCM	QCM	QCM-PR
3 (8-QAM)	29.2 dB	39.8 dB	39.2 dB
4 (16-QAM)	41.8 dB	40.6 dB	38.6 dB
5 (32-QAM)	45.5 dB	41.8 dB	40 dB
6 (64-QAM)	48.2 dB	43.7 dB	40.2 dB

TABLE III
COMPARISON OF E_b/N_0 REQUIRED BY DCM, QCM, AND QCM-PR TO ACHIEVE A BER OF 10^{-3} WITH M-QAM ALPHABETS.

B. DCM-OFDM

In this subsection, we present DCM-OFDM, its detection, and performance. In DCM-OFDM, complex OFDM symbols are transmitted through a dual-LED setup using intensity modulation. In DCM-OFDM transmitter, N complex symbols from $\mathbb{A}$ carrying $N \log_2 |\mathbb{A}|$ information bits are transformed by the IFFT matrix to get a $N \times 1$ vector of complex transmit symbols denoted as $\mathbf{s} = [s_1, s_2, \cdots, s_N]^T = \mathbf{F}^H \mathbf{v}$, where $\mathbf{v} = [v_1, v_2, \cdots, v_N]^T \in \mathbb{A}^N$. The elements of $\mathbf{s}$ are transmitted in N channel uses through the DCM transmitter.

1) Zero-forcing based DCM-OFDM signal detection: Let $\mathbf{Y} = [\mathbf{y}_1, \mathbf{y}_2, \cdots, \mathbf{y}_N]$ be the $N_r \times N$ matrix of received vectors corresponding to the $2 \times N$ matrix of transmit vectors $\mathbf{X} = [\mathbf{x}_1, \mathbf{x}_2, \cdots, \mathbf{x}_N]$. We can detect the transmitted complex values at the receiver by performing a zero-forcing (ZF) equalization for the channel matrix $\mathbf{H}$. That is, the transmitted vectors can be estimated as

$$\widehat{\mathbf{X}} = \frac{1}{a}(\mathbf{H}^T \mathbf{H})^{-1} \mathbf{H}^T \mathbf{Y}. \tag{19}$$

The N complex OFDM symbols can be reconstructed as

$$\hat{s}_i = \hat{x}_i(1) e^{j \hat{x}_i(2)}, \tag{20}$$

where $\hat{x}_i(k)$ is the kth element of the ith column vector in the matrix $\widehat{\mathbf{X}}$. Now, OFDM demodulation is preformed as $\hat{\mathbf{v}} = \mathbf{F}\hat{\mathbf{s}}$ and the $N \log_2 |\mathbb{A}|$ information bits are demapped from it. The complexity of ZF detector is $O(2N_r N)$.

2) Minimum distance detector: We saw in Sec. III-E3 that the minimum distance detector offers performance improvement over ZF detector for QCM-OFDM. Similarly, the performance of DCM-OFDM can be improved by using the minimum distance detector. Let $\mathbb{S}_{DO}$ be the set of all possible values of the DCM-OFDM transmit matrix $\mathbf{X}$, i.e., $\mathbf{X} \in \mathbb{S}_{DO}$ and $|\mathbb{S}_{DO}| = |\mathbb{A}^N|$. Thus, every matrix in $\mathbf{X} \in \mathbb{S}_{DO}$ corresponds to an $N \times 1$ complex vector $\mathbf{v} \in \mathbb{A}$. In the MD detector, $\mathbf{v}$ can be estimated as

$$\hat{\mathbf{v}} = \underset{\mathbf{X} \in \mathbb{S}_{DO}}{\arg\min} \| \mathbf{Y} - a\mathbf{H}\mathbf{X} \|. \tag{21}$$

The $N \log_2 |\mathbb{A}|$ information bits are demapped from $\hat{\mathbf{v}}$. The complexity of the MD detector is $O(|\mathbb{A}|^N)$.

3) BER performance of DCM-OFDM: The BER performance of DCM-OFDM scheme with $N = 8$ and 4-QAM using ZF and MD detectors is presented in Fig. 16. For comparison purpose, we have also plotted the performance of QCM-OFDM in Fig. 16. The simulation parameter settings are same as those listed in Table II. It can be observed that the MD detector outperforms ZF detector by about 8 dB at a BER of 10^{-5}. DCM-OFDM with MD detector outperforms QCM-OFDM with MD detector at lower to moderate SNR values. However, QCM-OFDM with ZF detector outperforms DCM-OFDM with ZF detector at all SNRs. The ZF detector performs well for QCM-OFDM due to the availability of the additional degrees of freedom in QCM.

V. PROPOSED SM-DCM SCHEME

The DCM scheme proposed in the previous section conveys the magnitude and phase of a complex symbol through two LEDs. The achieved rate can be increased through the use
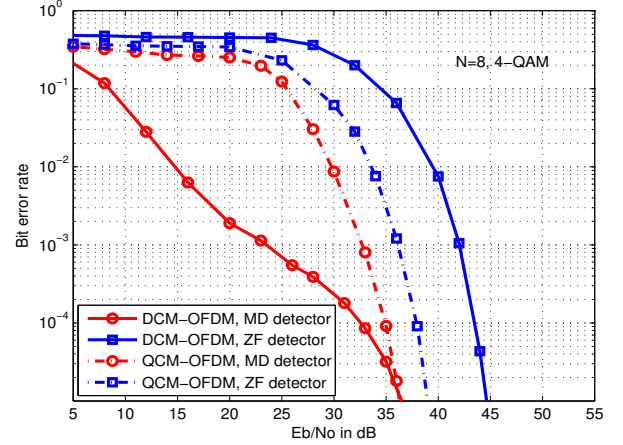

Fig. 16. BER performance of DCM-OFDM with ZF and MD detectors for $N = 8$ and 4-QAM.

of spatial modulation in DCM. The spatial modulation-DCM (SM-DCM) scheme proposed in this section is based on this idea. In the SM-DCM scheme, in addition to modulation bits, there are additional bits which are conveyed through spatial indexing. The DCM scheme restricts the number of LEDs to be two, whereas SM-DCM scheme allows the use of multiple pairs of LEDs. The proposed SM-DCM scheme uses two LEDs (one pair of LEDs) as one BLOCK to convey a complex symbol (just like in case of DCM). The number of BLOCKs (pairs of LEDs) is given by $N_p = \lfloor \frac{N_t}{2} \rfloor$. The selection of a BLOCK to use in a given channel use is done using index bits. The number of index bits for BLOCK selection is $\log_2 N_p$.

A. SM-DCM transmitter

The block diagram of SM-DCM transmitter is shown in Fig. 17. In this scheme, we consider $N_t = 4$. Therefore, the number of BLOCKs is, $N_p = 2$ (BLOCK 1 and BLOCK 2). After the data bits are mapped to a complex symbol (QAM/PSK), selection of the BLOCK to which this complex symbol is given as input is to be done. It is done by the index bits (in this case, it is one index bit, b) as follows.

$$\text{If } b = \begin{cases} 0, & \text{then } s \text{ goes to BLOCK 1} \\ 1, & \text{then } s \text{ goes to BLOCK 2}. \end{cases} \tag{22}$$

After the BLOCK selection is done, the process is same as that of the DCM scheme described in Sec. IV. If BLOCK 1 is selected, then LED1 transmits the magnitude (r) and LED2 transmits the phase (ϕ) of the complex symbol (s). Similarly, if BLOCK 2 is selected, then LED3 transmits the magnitude (r) and LED4 transmits the phase (ϕ) of the complex symbol (s). The definitions of r and ϕ are same as in DCM.

Example 3: If the complex modulation symbol to be transmitted is $s = 3 + j3$ and if the index bit is 0, then $r = 3\sqrt{2}$, $\phi = \frac{\pi}{4}$ and BLOCK 1 will be selected. LED1 emits light of intensity $3\sqrt{2}$ and LED2 emits light of intensity $\frac{\pi}{4}$. LED3 and LED4 will be OFF. The corresponding SM-DCM transmit vector is $\mathbf{x} = [3\sqrt{2} \ \frac{\pi}{4} \ 0 \ 0]^T$.

Example 4: If the complex modulation symbol to be transmitted is $s = 3 + j3$ and if the index bit is 1, then $r = 3\sqrt{2}$, $\phi = \frac{\pi}{4}$ and BLOCK 2 will be selected. LED3 emits light
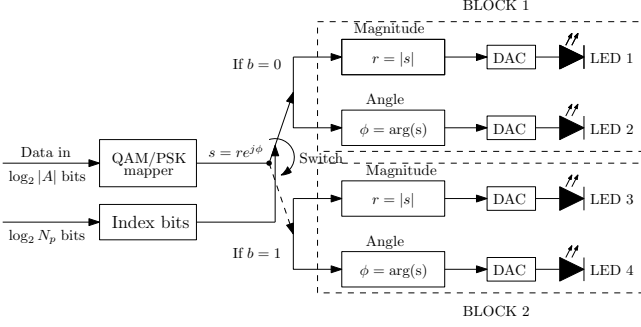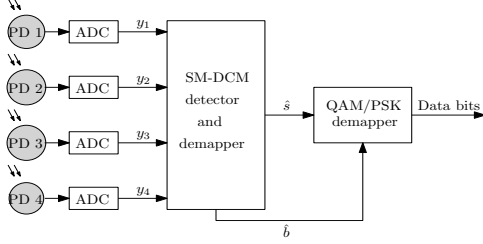
Fig. 17. SM-DCM transmitter.

Fig. 18. SM-DCM receiver.
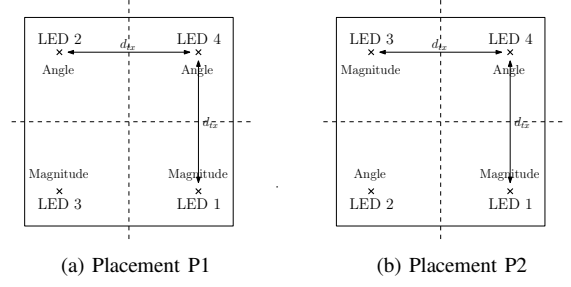

(a) Placement P1   (b) Placement P2

Fig. 19. Placement of LEDs for SM-DCM.

We choose the placement of LEDs such that $d_{min,\mathbf{H}}$ and $d_{avg,\mathbf{H}}$ in that placement are maximized. The placement of LEDs in Fig. 19 (a) and Fig. 19 (b) are considered as P1 and P2, respectively. We have computed values of $d_{min,\mathbf{H}}$, $d_{avg,\mathbf{H}}$ for placements P1, P2 and 8-QAM, 32-QAM for the SM-DCM scheme. The computed values are listed in Table IV. From this table, we observe that $d_{min,\mathbf{H}}$ and $d_{avg,\mathbf{H}}$ values are maximum for LED placement P2. So, we choose LED placement P2 (as in Fig. 19 (b)) in our simulation results for SM-DCM.

LED placement	Modulation	$d_{min,\mathbf{H}}$	$d_{avg,\mathbf{H}}$
P1	8-QAM	2.0420×10^{-14}	5.0340×10^{-10}
P2	8-QAM	8.5358×10^{-13}	5.0460×10^{-10}
P1	32-QAM	1.8470×10^{-14}	6.2289×10^{-10}
P2	32-QAM	9.2177×10^{-14}	6.2510×10^{-10}

TABLE IV
VALUES OF $d_{min,\mathbf{H}}$, $d_{avg,\mathbf{H}}$ FOR DIFFERENT PLACEMENTS AND M-QAM ALPHABETS OF SM-DCM.

of intensity $3\sqrt{2}$ and LED4 emits light of intensity $\frac{\pi}{4}$. LED1 and LED2 will be OFF. The corresponding SM-DCM transmit vector is $\mathbf{x} = [0 \ \ 0 \ \ 3\sqrt{2} \ \ \frac{\pi}{4}]^T$.

B. SM-DCM signal detection

The block diagram of SM-DCM receiver with $N_r = 4$ PDs is shown in the Fig. 18. Following the system model in Sec. II, the $N_r \times 1$ received signal vector at the output of the PDs is given by (3). Assuming perfect channel knowledge at the receiver, the ML estimate of the transmit vector $\mathbf{x}$ is obtained as

$$\hat{\mathbf{x}}_{ML} = \underset{\mathbf{x} \in \mathbb{S}_{SD}}{\operatorname{argmin}} \|\mathbf{y} - a\mathbf{H}\mathbf{x}\|^2, \qquad (23)$$

where $\mathbb{S}_{SD}$ denotes the SM-DCM signal set (consisting of all possible $\mathbf{x}$ vectors). The detected vector $\hat{\mathbf{x}}_{ML}$ is demapped to the corresponding complex symbol $\hat{s}_{ML}$, which is then demapped to get the corresponding modulation bits. By looking at the non-zero indices of the detected vector $\hat{\mathbf{x}}_{ML}$, we can detect the index bits $\{\hat{b}\}$.

Achieved rate in SM-DCM: The achieved rate in DCM is $\log_2|\mathbb{A}|$ bpcu. It is increased by $\log_2 N_p$ due to index bits in SM-DCM. Thus, the achieved rate in SM-DCM is given by

$$\eta_{smdcm} = \log_2|\mathbb{A}| + \log_2 N_p \text{ bpcu.} \qquad (24)$$

C. Optimum placement of LEDs for SM-DCM

Several LED placements are possible for SM-DCM. We use two metrics, namely, minimum Euclidean distance and average Euclidean distance between any two SM-DCM signal vectors $\mathbf{x}_1$ and $\mathbf{x}_2$ transmitted through $\mathbf{H}$ (i.e., $d_{min,\mathbf{H}}$ and $d_{avg,\mathbf{H}}$), to decide the optimum placement of LEDs for SM-DCM. The definitions of $d_{min,\mathbf{H}}$ and $d_{avg,\mathbf{H}}$ are given below:

$$d_{min,\mathbf{H}} \triangleq \underset{\mathbf{x}_1, \mathbf{x}_2 \in \mathbb{S}_{SD}}{\operatorname{argmin}} \ \|\mathbf{H}(\mathbf{x}_2 - \mathbf{x}_1)\|^2, \qquad (25)$$

$$d_{avg,\mathbf{H}} \triangleq \frac{1}{\binom{|\mathbb{S}_{SD}|}{2}} \sum_{\mathbf{x}_1, \mathbf{x}_2 \in \mathbb{S}_{SD}} \|\mathbf{H}(\mathbf{x}_2 - \mathbf{x}_1)\|^2. \qquad (26)$$

D. BER performance of SM-DCM

An upper bound on the BER of QCM for ML detection was obtained in Sec. III-C1. In a similar way, an upper bound on the BER of SM-DCM can be obtained. Figure 20 shows the upper bound and simulated BER plots for SM-DCM with ML detection at 8-QAM and 32-QAM. The system parameters used are the same as in Table II. The placement of LEDs used for the simulations of SM-DCM is specified in Fig. 19 (b), and $d_{tx} = 1$m. It can be seen that the upper bound is tight at moderate to high SNRs. In the next section (Sec. VI), we use this tight bound on BER to compute the achievable rate contours in SM-DCM.

Figure 21 presents a comparison of the BER performance of QCM, DCM, and SM-DCM with ML detection for $\eta = 4$ and 6 bpcu. For the DCM plots, LED1 and LED2 in Fig. 19 (b) are considered. From Fig. 21, we observe that for $\eta = 4$ bpcu, QCM and DCM require 16-QAM whereas SM-DCM requires 8-QAM only, which is why SM-DCM performs better by about 3 dB and 7 dB at 10^{-4} BER compared to QCM and DCM, respectively. Similarly, for $\eta = 6$ bpcu, SM-DCM performs better than DCM by about 4 dB, since DCM requires 64-QAM whereas SM-DCM requires 32-QAM only. For $\eta = 6$ bpcu, QCM performs better by about 10 dB and 5 dB at 10^{-4} BER compared to DCM and SM-DCM, respectively. In case of QCM and SM-DCM for $\eta = 6$ bpcu, SM-DCM performs better at low E_b/N_0 because of lower QAM size
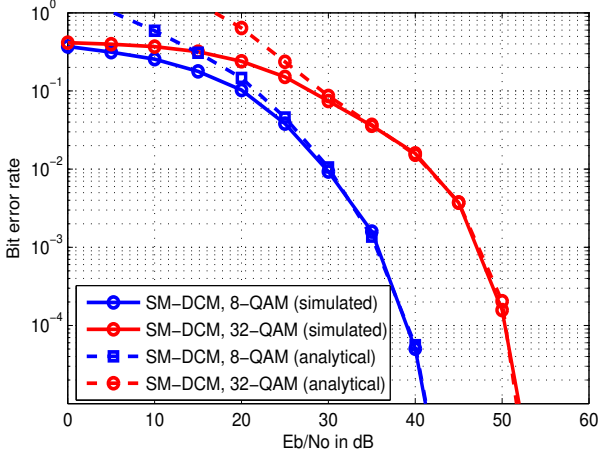
Fig. 20. Comparison of analytical upper bound and simulated BER for SM-DCM with 8-QAM and 32-QAM.
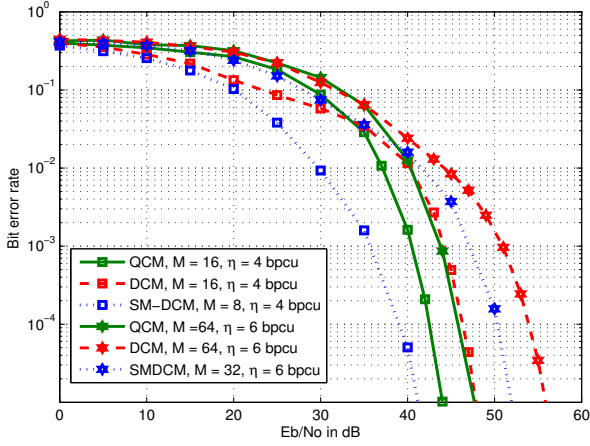

Fig. 21. Comparison of BER performance of QCM, DCM, and SM-DCM for $\eta = 4, 6$ bpcu.

whereas QCM performs better at high E_b/N_0, because of the same reason as explained in Sec. IV-A. That is, for large QAM sizes, the average relative distance between the transmit vectors in QCM is more compared to that in SM-DCM, i.e., if $(\mathbf{x}_i, \mathbf{x}_j)$, $i \neq j$, is a pair of vectors from the transmit signal set, then $\mathbb{E}[\|\mathbf{x}_i - \mathbf{x}_j\|]$ is larger for the QCM signal set than for the SM-DCM signal set.

VI. SPATIAL DISTRIBUTION OF SNR AND ACHIEVABLE RATE CONTOURS

In addition to the BER vs E_b/N_0 performance plots presented in the previous chapters, spatial characterization of the achieved performance in the proposed QCM, DCM, and SM-DCM schemes is of interest. To address this need, in this section we study i) the spatial distribution of average received SNR ($\bar{\gamma}$ defined in Sec. II), ii) achievable rate contours for a given target BER, and iii) percentage area of the room covered for a given rate and target BER in QCM, DCM, and SM-DCM. The system parameters used in the computation of the above quantities are as in Table II. Additional system parameters are listed in Table V. The LEDs placement and

Parameter	Description	Value
q	Charge of an electron	1.602×10^{-19} C
I_a	Ambient light photo current	5.84 mA
I_2	Noise bandwidth factor	0.562
T	Signaling interval	0.05 μsec
B_a	Photo diode amplifier bandwidth	50 MHz
ρ	Photo diode amplifier noise density	5pA/$\sqrt{\text{Hz}}$

TABLE V
SYSTEM PARAMETERS FOR COMPUTATION OF NOISE POWER.

the signal mapping to LEDs for QCM and DCM are as in the Fig. 4. The LEDs placement and the signal mapping to LEDs for SM-DCM are as in the Fig. 19. The output power of each LED is 1 Watt. We compute the average received SNRs at various spatial points on the plane of the receiver at a spatial resolution of 2.5 cm. To compute the noise power at the receiver, we use the following expression given in [28] and use the parameter values used therein (which are summarized in Table V):

$$\sigma^2 = 2qa(P_r + I_a/a)I_2/T + B_a\rho^2. \quad (27)$$

We consider a target BER of 10^{-5}. Note that Figs. 5, 14, and 20 demonstrated the tightness of the BER upper bounds obtained in Secs. III-C, IV-A, and V-D for QCM, DCM, and SM-DCM, respectively. Indeed, the upper bounds and simulation results almost match for BERs below 10^{-3}. Therefore, these bounds can be used to accurately map the spatial distribution of the SNRs to achievable rate contours for the considered target BER of 10^{-5}. This is done as follows. Using the average received SNR at a given spatial position of the receiver and the BER vs SNR relation given by the BER upper bound expression, determine the maximum QAM size (among 2-, 4-, 8-, 16-, 32-, 64-QAM) that meets the 10^{-5} BER target. This determination is made for all spatial positions of the receiver at a spatial resolution of 2.5cm. The resulting spatial map of the maximum QAM size possible gives the achievable rate in bpcu at various spatial positions of the receiver.

Results and discussions: We computed the spatial performance measures discussed above for QCM, DCM, and SM-DCM with $d_{tx} = 2$m and $\Phi_{\frac{1}{2}} = 60°$. Figures 22(a),(b), and (c) show these performance plots for QCM, DCM, and SM-DCM, respectively. It can be observed that the maximum rate achieved by QCM and SM-DCM while meeting the 10^{-5} BER target is 5 bpcu (i.e., maximum supported QAM size is 32-QAM and 16-QAM for QCM and SM-DCM, respectively) and the maximum rate achieved by DCM is 4 bpcu (i.e., maximum supported QAM size is 16-QAM). This is due to the observation we made in Fig. 15 and 21, where we saw that QCM had a larger average relative distance between the transmit vectors compared to DCM and SM-DCM for large QAM sizes and this resulted in a favorable performance for QCM over DCM and SM-DCM. This is found to result in QCM achieving a larger percentage area of the room covered by 4 bpcu (covering 70% area) and 5 bpcu (covering 45% area) rates than DCM. Similarly, QCM achieves a larger percentage area of the room covered by 5 bpcu (covering 70% area) than SM-DCM. DCM shows a performance advantage over QCM for 8-QAM; this can be seen by observing that
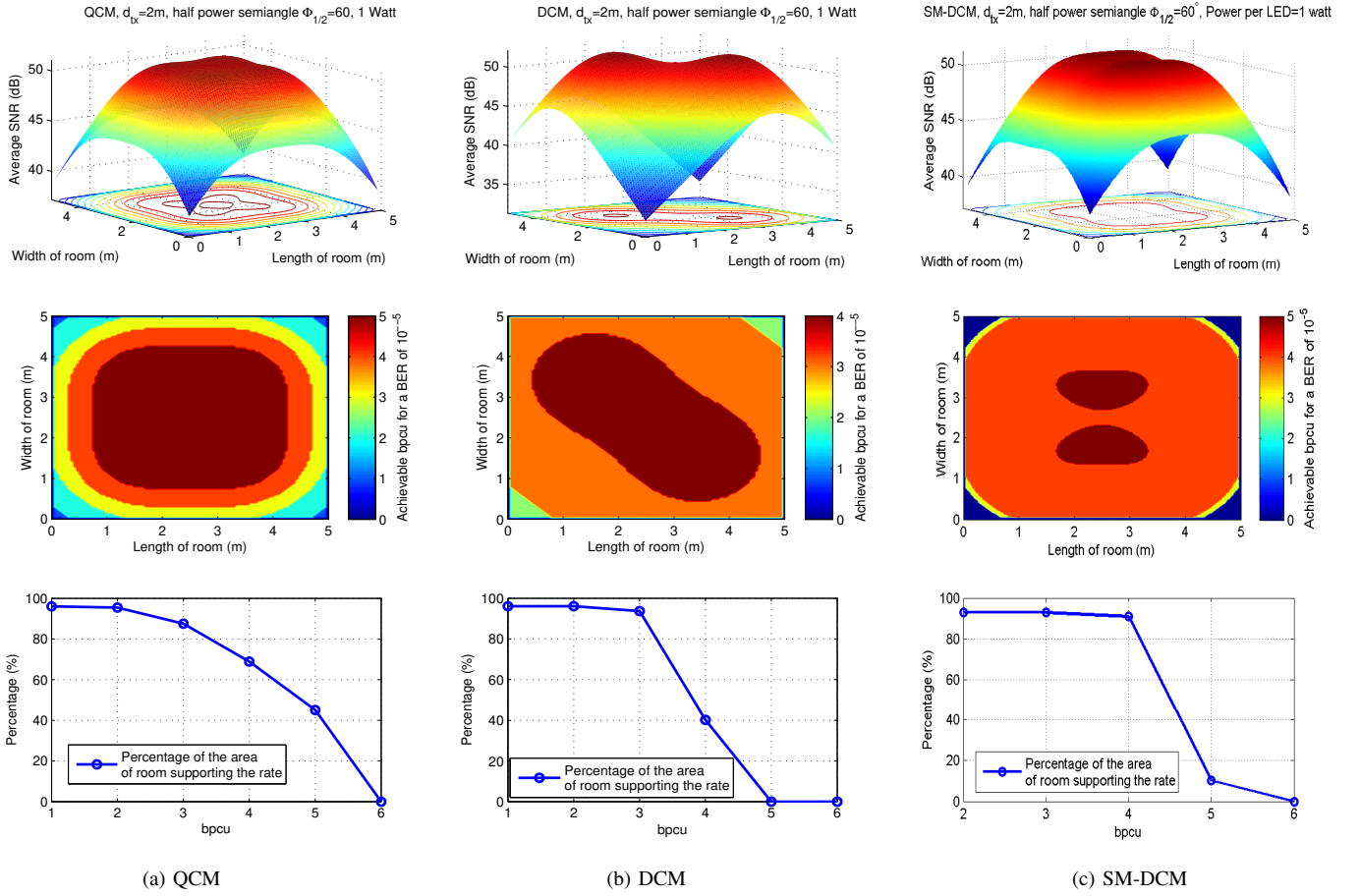
Fig. 22. Plots of spatial distribution of average received SNR, achievable rate contours for 10^{-5} BER, and percentage area of the room covered vs achieved rate for (a) QCM, (b) DCM, and (c) SM-DCM.

DCM supports 8-QAM in more than 90% of the room while QCM covers a lesser area for 8-QAM. Similarly, SM-DCM shows a performance advantage over QCM and DCM for $\eta = 3, 4$ bpcu and $\eta = 4$ bpcu, respectively. This can be seen by observing that SM-DCM covers more than 90% of the room while QCM and DCM covers a lesser area for $\eta = 3, 4$ bpcu and $\eta = 4$ bpcu, respectively.

VII. CONCLUSIONS

We proposed three simple and novel complex modulation schemes that avoided the Hermitian symmetry operation to generate LED compatible positive real signals encountered in VLC. This was achieved through the exploitation of the spatial dimension for the purpose of complex symbol modulation. In the proposed QCM scheme, four LEDs were used to convey the real and imaginary parts of a complex symbol and their sign information. While intensity modulation of LEDs was employed to convey the magnitudes of the real and imaginary parts, spatial index modulation of LEDs was used to convey their sign information. The proposed DCM scheme, on the other hand, exploited the polar representation of complex symbols to use only two LEDs to convey the magnitude and phase information of a complex symbol. The proposed SM-DCM scheme exploited the use of spatial modulation in DCM. Analytical upper bounds and simulation results showed

that the proposed QCM, DCM, and SM-DCM achieve good BER performance. Phase rotation of modulation symbols was shown to improve the BER performance in QCM. Zero-forcing and minimum distance detectors for QCM and DCM when used along with OFDM showed good performance for these QCM-OFDM and DCM-OFDM schemes. The analytical BER upper bounds were shown to be very tight at high SNRs, and this enabled us to easily compute and plot the achievable rate contours for a given target BER (e.g., 10^{-5} BER) in QCM, DCM, and SM-DCM.

REFERENCES

[1] H. Elgala, R. Mesleh, and H. Haas, "Indoor optical wireless communication: potential and state-of-the-art," *IEEE Commun. Mag.*, vol. 49, no. 9, pp. 56-62, Sep. 2011.

[2] D. O'Brien, "Visible light communications: challenges and potential," *Proc. IEEE Photon. Conf.*, pp. 365-366, Oct. 2011.

[3] T. Q. Wang, Y. A. Sekercioglu, and J. Armstrong, "Analysis of an optical wireless receiver using a hemispherical lens with application in MIMO visible light communications," *J. Lightwave Tech.*, vol. 31, no. 11, pp. 1744-1754, Jun. 2013.

[4] T. Fath and H. Haas, "Performance comparison of MIMO techniques for optical wireless communications in indoor environments," *IEEE Trans. Commun.*, vol. 61, no. 2, pp. 733-742, Feb. 2013.

[5] N. A. Tran, D. A. Luong, T. C. Thang, and A. T. Pham, "Performance analysis of indoor MIMO visible light communication systems," *Proc. IEEE ICCE 2014*, pp. 60-64, Jul. 2014.

[6] Y. Gong, L. Ding, Y. He, H. Zhu, and Y. Wang, "Analysis of space shift keying modulation applied to visible light communications," *Proc. IETICT 2013*, pp. 503-507, Apr. 2013.

[7] W. O. Popoola, E. Poves, and H. Haas, "Error performance of generalised space shift keying for indoor visible light communications," *IEEE Trans. Commun.*, vol. 61, no. 5, pp. 1968-1976, May 2013.

[8] R. Mesleh, R. Mehmood, H. Elgala, and H. Haas, "Indoor MIMO optical wireless communication using spatial modulation," *Proc. IEEE ICC 2010*, pp. 1-5, May 2010.

[9] S. P. Alaka, T. Lakshmi Narasimhan, A. Chockalingam, "Generalized spatial modulation in indoor wireless visible light communication," *Proc. IEEE GLOBECOM 2015*, Dec. 2015.

[10] P. Butala, H. Elgala, and T. D. C. Little, "Performance of optical spatial modulation and spatial multiplexing with imaging receiver," *Proc. IEEE WCNC 2014*, Apr. 2014.

[11] J. Armstrong, "OFDM for optical communications," *J. Lightwave Tech.*, vol. 27, no. 3, pp. 89-204, Feb. 2009.

[12] O. Gonzlez, R. Prez-Jimnez, S. Rodriguez, J. Rabadn, and A. Ayala, "OFDM over indoor wireless optical channel," *Proc. IEE Optoelectron.*, vol. 152, no. 4, pp. 199-204, Aug. 2005.

[13] H. Elgala, R. Mesleh, H. Haas, and B. Pricope, "OFDM visible light wireless communication based on white LEDs," *Proc. IEEE VTC 2007-Spring*, pp. 2185-2189, Apr. 2007.

[14] A. H. Azhar, T. A. Tran, and D. O'Brien, "A gigabit/s indoor wireless transmission using MIMO-OFDM visible-light communications," *IEEE Photonics Tech. Lett.*, vol. 25, no. 2, pp. 171-174, Dec. 2013.

[15] H. Elgala, T. D. C. Little, "SEE-OFDM: Spectral and energy efficient OFDM for optical IM/DD systems," *Proc. IEEE PIMRC 2014*, Sep. 2014.

[16] J. Armstrong and A. J. Lowery, "Power efficient optical OFDM," *Electron. Lett.*, vol. 42, no. 6, pp. 370-372, Mar. 2006.

[17] J. Armstrong and B. J. Schmidt, "Comparison of asymmetrically clipped optical OFDM and DC-biased optical OFDM in AWGN," *IEEE Commun. Lett.*, vol. 12, no. 5, pp. 343-345, May 2008.

[18] N. Fernando, Y. Hong, and E. Viterbo, "Flip-OFDM for optical wireless communications," *Proc. IEEE ITW 2011*, pp. 5-9, Oct. 2011.

[19] N. Fernando, Y. Hong, and E. Viterbo, "Flip-OFDM for unipolar communication systems," *IEEE Trans. Commun.*, vol. 60, no. 12, pp. 3726-3733, Aug. 2012.

[20] A. Nuwanpriya, A. Grant, S. W. Ho, and L. Luo, "Position modulating OFDM for optical wireless communications," *Proc. IEEE GLOBECOM 2012 Workshop*, pp. 1219-1223, Dec. 2012.

[21] Y. Li, D. Tsonev, and H. Haas, "Non-DC-biased OFDM with optical spatial modulation," *Proc. IEEE PIMRC 2013*, pp. 486-490, Sep. 2013.

[22] S. P. Alaka, T. Lakshmi Narasimhan, and A. Chockalingam, "Coded index modulation for non-DC-biased OFDM in multiple LED visible light communication," *Proc. IEEE VTC'2016-Spring*, May 2016.

[23] R. Tejaswi, T. Lakshmi Narasimhan, and A. Chockalingam, "Quad-LED complex modulation (QCM) for visible light wireless communication," *Proc. IEEE WCNC'2016 Workshops*, Apr. 2016.

[24] R. Tejaswi, *Multiple-LED Complex Modulation Schemes for Visible Light Communication*, M.E. Thesis, Department of ECE, Indian Institute of Science, Bangalore, June 2016.

[25] D. Tse and P. Viswanath, *Fundamentals of Wireless Communication,* Cambridge Univ. Press, 2005.

[26] J. Barry, J. Kahn, W. Krause, E. Lee, and D. Messerschmitt, "Simulation of multipath impulse response for indoor wireless optical channels," *IEEE J. Sel. Areas in Commun.*, vol. 11, no. 3, pp. 367-379, Apr. 1993.

[27] F. R. Gfeller and U. Bapst, "Wireless in-house data communication via diffuse infrared radiation," *Proceedings of the IEEE*, vol. 67, no. 11, pp. 1474-1486, Nov. 1979.

[28] L. Zeng, D. O'Brien, H. Le Minh, K. Lee, D. Jung, and Y. Oh, "Improvement of date rate by using equalization in an indoor visible light communication system," *Proc. IEEE ICCSC 2008*, pp. 678-682, May 2008.

[29] J. M. Kahn and J. R. Barry, "Wireless infrared communications," *Proceedings of the IEEE*, vol. 85, no. 2, pp. 265-298, Feb. 1997.

[30] S. Verdu, *Multiuser detection*, Cambridge Univ. Press, 1998.